Hydrophobic Core Mutations in CI2 Globally Perturb Fast Side-Chain Dynamics Similarly without Regard to Position

Matthew J. Whitley[‡], **Jun Zhang**[‡], and **Andrew L. Lee**[‡,§,*]

[‡]*Department of Biochemistry & Biophysics, School of Medicine, University of North Carolina at Chapel Hill, Chapel Hill, NC 27599*

[§]*Division of Medicinal Chemistry & Natural Products, School of Pharmacy, University of North Carolina at Chapel Hill, Chapel Hill, NC 27599*

Abstract

Protein dynamics is currently an area of intense research because of its importance as complementary information to the huge quantity of available data relating protein structure and function. Because it is usually the influence of dynamics on function that is studied, the physical determinants of the distribution of flexibility in proteins have not been explored as thoroughly. In the present NMR study, an expanded suite of five ^2H relaxation experiments was used to characterize the picosecond-nanosecond side-chain dynamics of chymotrypsin inhibitor 2 (CI2) and five hydrophobic core mutants, some of which are members of the folding nucleus. Because CI2 is a homologue of the serine protease inhibitor eglin c, which has already been extensively characterized in terms of its dynamics, it was possible to compare not only side-chain dynamics, but also the *responses* of these dynamics to analogous mutations. Remarkably, each of the five core mutations in CI2 led to similar and reproducible increases in side-chain flexibility throughout the entire structure. Although the expanded suite of ^2H relaxation experiments does not affect model selection for the vast majority of residues, it did enable the detection of increasing levels of nanosecond-scale motions in CI2's reactive site binding loop as the L68 side chain was progressively shortened by mutation. Collectively, we observed that the CI2 mutants are more dynamically similar to each other than to the more rigid wild-type CI2, from which we conclude that wild-type CI2 has been optimized to a specific level of rigidity which may aid in its function as a serine protease inhibitor. We also observed that the pattern of side-chain dynamics of CI2 is quantitatively similar to eglin c, but that this similarity is lost upon mutating both proteins at an equivalent position. Finally, ^{15}N relaxation was used to characterize the backbone dynamics of wild-type and mutant CI2. Interestingly, mutation at folding nucleus positions led to widespread increases in backbone flexibility, whereas non-folding-nucleus positions led to increases in flexibility in the C-terminal half of the protein only.

Keywords

NMR; CI2; hydrophobic cores; side-chain dynamics; ^2H relaxation; ^{15}N relaxation; homologous proteins

The realization that internal dynamics across multiple time scales can impact both protein thermodynamics and function to a significant degree has changed the conceptual framework for phenomena such as catalysis and signal transduction. Motions in the picosecond-

[*]To whom correspondence should be addressed: University of North Carolina, Division of Medicinal Chemistry & Natural Products, School of Pharmacy, Beard Hall 201, CB# 7360, Chapel Hill, NC 27599-7360. Email: drewlee@unc.edu. Phone: (919) 966-7821. Fax: (919) 843-5150.

nanosecond (ps-ns) time regime impact a protein's thermodynamics via contributions to its conformational entropy and thus total free energy (1-10), while slower motions taking place on the microsecond-to-millisecond (μs-ms) time scale have typically been linked to allostery (11,12) and enzymatic catalysis (13,14). Less well understood, however, are the physical determinants of protein internal motions, especially side-chain dynamics. Efforts to predict internal dynamics based on structure have shown promise (15,16), but the moderate correlations observed in such attempts indicate that more than one or a few different factors must come into play.

In this study, we employ a range of sophisticated NMR methodologies to characterize the dynamical consequences of five hydrophobic core mutations in chymotrypsin inhibitor 2 (CI2), a 7.3 kDa serine protease inhibitor from barley seeds (17,18). The five core mutants studied (L68V, L68A, I76V, V28A, and V66A) were selected to increase understanding of several specific issues concerning internal dynamics in hydrophobic cores (Figure 1). Residues L68 and I76 are known members of the CI2 folding nucleus, as determined by both experimental Φ-value analysis (19) and computational approaches (20,21). We sought to determine whether these residues, which make important contacts that stabilize the transition state during folding, are also important for modulating CI2's internal dynamics in the native state. Furthermore, computational studies of CI2 have suggested that L68 is one of two key energetic "linchpins" connecting CI2's hydrophobic core to its reactive loop (22). For this reason, we have selected two L68 mutants in which the length of the side chain is progressively reduced (L→V→A) in order to determine whether the dynamical character of the L68 side chain has a role in mediating this connection. V28 is not part of the canonical CI2 folding nucleus but is located near both L68 and I76 in the hydrophobic core, and thus was chosen to reveal whether residues proximal to canonical folding nuclei show similar dynamical behavior. V66, on the other hand, is neither part of the folding nucleus nor pointed into the same cluster of core residues formed by L68, I76, and V28. Analyzing the dynamical consequences of mutating this position adds perspective for interpreting the results of mutation to the canonical core residues. As a whole, the selected core mutations differ in location, the chemical identity of the WT residue, and the degree of severity of the mutation (although all are generally conservative), and differences between the dynamics of these mutants and WT CI2 should yield information on the relative contribution of each position to modulating the observed dynamics of the WT protein. Furthermore, the acquisition of the dynamics data for WT CI2 and hydrophobic core mutants will also allow us to compare the internal dynamics of CI2 to data available for the homologue eglin c.

Experimental Procedures

Protein Expression and Purification

Crystallographic evidence indicates that the first 19 amino acids of CI2 are unstructured (17). Consequently, experimental and computational studies of CI2 are routinely performed on a Δ1-19 truncation with residue 20 replaced by methionine, as is the case in the present work. WT CI2 DNA was generated from synthetic oligonucleotides using PCR and placed into the pET28a plasmid (Novagen). CI2 mutants were created by application of site-directed mutagenic PCR to the pET28a vector containing the WT sequence. Proteins were expressed in *E. coli* BL21 (DE3) cells (Invitrogen) grown at 37 °C to an optical density at 600 nm of 0.6-0.8 in 1 L of M9 minimal medium supplemented with 50 μg/mL kanamycin and containing 99%-^{15}NH$_4$Cl, U-^{13}C-glucose, and up to 60% ^{2}H$_2$O (v/v) as required for particular NMR samples. Expression was induced by addition of IPTG to a final concentration of 1 mM and allowed to proceed for 4-4.5 hours at 37 °C in a rotary shaker. The cells were harvested by centrifugation at 6,000 *g* for 30 min, and the cell pellet was resuspended in 40 mL of Buffer A (25 mM Tris·HCl, pH 8) and stored at -20 °C until needed. Frozen cell suspensions were

subjected to 3 rounds of freeze-thawing in a dry ice/ethanol bath, and cell lysis was completed by sonicating the sample 4×4 minutes. Cell debris from sonication was cleared by centrifugation at 20,000 g for 30 min, contaminant DNA was precipitated from the solution by the addition of polyethyleneimine to a final concentration of 0.2% (w/v), and the entire solution was allowed to stir on ice for 30 min. DNA was cleared from solution by centrifugation for 30 min at 20,000 g. The protein solution was then dialyzed overnight against 4 L of Buffer A. Chromatographic purification of CI2 was achieved by passing the dialyzed protein solution over an anion exchange column packed with Q-Sepharose FF resin (GE Healthcare) equilibrated in Buffer A and eluted by a linear gradient of Buffer B (2 M NaCl, 25 mM Tris·HCl, pH 8). Fractions containing CI2 (judged by the absorbance at 280 nm) were pooled, concentrated, and passed through a size-exclusion column consisting of Sephadex G-50 Superfine beads (GE Healthcare) equilibrated in NMR Buffer (20 mM KPO_4, 50 mM KCl, 0.02% NaN_3, pH 7). Pure CI2-containing fractions were again pooled, concentrated, and stored at -20 °C until needed. Typically, a 1 L culture yielded approximately 60 mg of pure protein.

NMR Resonance Assignments

Resonance assignment experiments were carried out on an 11.7 T Varian INOVA spectrometer equipped with a triple-resonance probe and z-axis pulsed field gradients using uniformly $^{13}C,^{15}N$-enriched CI2 samples in NMR Buffer (10% D_2O) at pH 7. Protein concentrations were 1-2 mM. Resonance assignments for the C_α, C_β, N, and H_N atoms of the non-proline residues of each CI2 variant were obtained using gradient-enhanced 3D HNCACB and CBCA(CO)NH experiments (23). The chemical shifts of side-chain methyl carbons (for A, V, L, I, and T) were assigned using the (H)CCH$_3$-TOCSY experiment (24), while methionine methyl carbons were assigned using a ^{1}H-^{13}C HMBC experiment in conjunction with the other assignment experiments. The prochirality of each side-chain methyl carbon was determined using a 10% ^{13}C-labeled sample (25) in conjunction with standard constant-time ^{1}H-^{13}C HSQCs. All spectra were processed using NMRPipe/NMRDraw (26) and analyzed using NMRView (27).

NMR Relaxation Experiments

The backbone ^{15}N T_1 and T_2 relaxation time constants and the ^{1}H-^{15}N heteronuclear NOE were measured at 25 °C with standard experiments (28) on 11.7 T and 14.4 T Varian INOVA spectrometers equipped with triple resonance probes and z-axis pulsed field gradients. The experimental samples consisted of 2 mM uniformly ^{15}N-labeled CI2 at pH 7 in 10% D_2O NMR Buffer. For WT and L68A, the T_1, T_2, and NOE experiments were performed twice at each field strength on samples originating from independent protein expressions in order to verify the reproducibility of the experimental data. For each relaxation experiment, peak intensities as a function of relaxation time were fitted to a monoexponential decay to yield the T_1 and T_2 time constants. Error estimates for the T_1 and T_2 data were made using three duplicate relaxation delay times in each experiment, whereas the error in the calculated heteronuclear NOEs was conservatively estimated as twice the RMSD of the spectral noise. After using the backbone relaxation data to determine the global tumbling time (τ_m) of each variant and to check for the existence of rotational anisotropy, Lipari-Szabo "model free" dynamics parameters (29) for each residue were extracted using the program relxn2.2 (30) by fitting the experimental ^{15}N data to one of five common forms of the spectral density function (31). The appropriate form of the spectra density function was selected on a per-residue basis by calculating both Akaike's information criterion (AIC) and the Bayesian information criterion (BIC) (32). For the very few cases in which the AIC and BIC recommended different forms of the spectral density, the simpler form was selected.

The ps-ns dynamics of the methyl-bearing side chains of WT and mutant CI2 were characterized at 25 °C by monitoring the relaxation as a function of time of the following five

types of ^{2}H coherence (33,34): transverse in-phase (D_+), longitudinal (D_z), transverse antiphase (AP), double quantum (DQ), and quadrupolar order (QO). ^{2}H relaxation experiments for each CI2 variant were conducted using samples of 2 mM CI2 uniformly labeled with ^{15}N and ^{13}C and 60% randomly labeled with ^{2}H in 10% D_2O NMR Buffer (pH 7) on the same spectrometers used for the ^{15}N relaxation measurements. Only signals from -CH$_2$D isotopomers could be detected in these experiments. The transverse and longitudinal relaxation time constants were measured at both 11.7 and 14.4 T, while the AP, DQ, and QO time constants were measured only at 11.7 T. As for the ^{15}N data, the error in each ^{2}H time constant measurement was estimated using three duplicate relaxation delays. To further verify the consistency of the data, measurements of the in-phase transverse and longitudinal time constants were repeated on separately prepared samples at both field strengths for both WT CI2 and L68A. As for the ^{15}N data, peak intensities as a function of time for each ^{2}H relaxation experiment were fitted to a monoexponential decay to extract the associated relaxation time constant. Raw DQ time constants were then corrected according to the method of Millet *et al.* (34) to yield estimates of the pure DQ time constants. The seven individual ^{2}H relaxation measurements for each residue and the overall global tumbling time τ_m derived from the ^{15}N relaxation measurements were then used to calculate model free dynamics parameters for each CI2 variant using the in-house program relxD (based on relxn2.2). RelxD generates "model free" parameters by fitting the data for each methyl group to two-parameter and three-parameter forms of the model free spectral density function. The statistical F-test was then used to determine whether the three-parameter model more accurately describes the experimental data, with $\alpha = 0.05$.

CI2 Structural Characterization

To elucidate the mutations' effects on CI2 backbone structure, N-H$_N$ and C$^\alpha$-H$^\alpha$ residual dipolar couplings (RDCs) were measured using stretched 6% polyacrylamide gels (35) as the macromolecular alignment medium. A 2D IPAP-based experiment (36) was used to measure N-H$_N$ crosspeak splittings in the absence and presence of macroscopic alignment, with the RDC value being the difference between the aligned and isotropic splitting values. C$^\alpha$-H$^\alpha$ RDCs were measured analogously using a 3D HNCA-based spectrum (37). RDC measurements were carried out at 25 °C on an 11.7 T Varian INOVA spectrometer using 1-2 mM CI2 samples in 10% D_2O NMR Buffer at pH 7. To verify the quality of each variant's measured RDCs, the program REDCAT (38) was used to compare the experimental values to values back-calculated from a high resolution WT CI2 crystal structure (PDB 2CI2).

To probe changes in side-chain structure, NMR measurements of the three-bond scalar couplings (39,40) between γ-methyl groups and their respective backbone amide nitrogens and carbonyl carbons ($^3J_{NC}$ and $^3J_{CC'}$) were used to calculate χ_1 rotamer populations (41,42) for V, I, and T residues in the CI2 variants under study. Errors in determining the ^3J values were estimated using the RMSD of the experimental noise. The experiments were carried out at 25 °C on samples containing 2 mM uniformly ^{13}C,^{15}N-labeled CI2 in 10% D_2O NMR buffer at pH 7 using an 11.7 T Varian INOVA spectrometer equipped with a cryogenic probe and *z*-axis pulsed field gradients.

Results and Discussion

Mutation of Folding Nuclei Affects Backbone Dynamics More Universally than Non-Folding-Nucleus Mutations

In addition to WT CI2, we studied the backbone dynamics of five CI2 mutants. Mutants L68V, L68A, and I76V were chosen because they belong to the canonical CI2 folding nucleus. V28A and V66A are not members of the folding nucleus, but are located in proximity to it and were selected to provide context for interpreting the results of mutating folding nucleus residues. As

a reference, the average T_1 values at 500 MHz for non-reactive-loop residues in WT, L68V, L68A, I76V, V28A, and V66A were, respectively, 0.393±0.010, 0.387±0.003, 0.389±0.003, 0.396±0.003, 0.388±0.004, and 0.395±0.002 seconds. For T_2, the averages of the 500 MHz data excluding reactive loop residues were 0.175±0.002, 0.170±0.001, 0.170±0.001, 0.165 ±0.003, 0.166±0.002, and 0.166±0.001 seconds. The respective 500 MHz NOE averages were 0.693±0.005, 0.698±0.004, 0.696±0.008, 0.699±0.007, 0.691±0.012, and 0.694±0.010. Based on the ^{15}N T_1, T_2, and heteronuclear NOE measurements of rigid backbone amides at two static magnetic field strengths, the globally-optimized tumbling times (τ_m) for WT CI2, L68V, L68A, I76V, V28A, and V66A, were respectively calculated to be 4.05 ns, 4.13 ns, 4.10 ns, 4.29 ns, 4.07 ns, and 4.25 ns. Because the results of the Lipari-Szabo dynamics analysis are influenced by the type of rotational diffusion a macromolecule undergoes (43), we used the ^{15}N data for WT CI2 and L68A to check for the presence of rotational diffusion anisotropy. The ratio $D_{\parallel}/D_{\perp}$ for WT CI2 and L68A, calculated using the local diffusion constant approach (44), was 1.09 and 1.12, respectively, suggesting that the use of an isotropic rotational diffusion tensor is appropriate; fitting the WT data to an axially symmetric diffusion model resulted in no significant changes in extracted dynamics parameters (data not shown). Furthermore, since the mutations studied are generally isolated from solvent and thus not expected to exert a significant influence on the mutants' hydrodynamic properties, the ^{15}N relaxation data for all CI2 variants were analyzed using the isotropic rotational diffusion model.

Fitting the ^{15}N T_1, T_2, and heteronuclear NOE measurements for WT CI2 and each mutant to the Lipari-Szabo "model free" formalism yields on a per-residue basis the parameters S^2 and τ_e, which, respectively, provide information on the amplitude and correlation time on the ps-ns time scale of the motion of a particular internuclear vector, in this case the vector between the amide nitrogen and the amide proton. The parameter S^2 ranges from 0 to 1, with a value of 1 representing a completely rigid vector and a value of 0 indicating a bond vector undergoing isotropic reorientation, while the value of τ_e is ideally greater than one order of magnitude faster than overall rotational diffusion. The S^2 data for each mutant were compared to the WT by further calculating $\Delta S^2 = S^2_{\text{mutation}} - S^2_{WT}$ for each residue; we consider significant changes to be those for which the magnitude of ΔS^2 is at least twice that of the propagated error. These data can be seen in Figure 2. For all mutants, one overall trend is immediately obvious, namely that most of the ΔS^2 values are negative, indicating that the backbones of the mutant proteins are slightly more flexible than the WT main chain. This effect, however, is small, as most of the changes are less than -0.05 and very few reach -0.1.

More interesting than the magnitude of changes is the pattern of backbone dynamics changes. The two non-folding-nucleus mutants (V66A, V28A) show virtually no backbone perturbations in their N-terminal half (approximately to residue 46). In contrast, the folding nucleus mutants (L68V, L68A, I76V) show increases in backbone flexibility, many of them significant, in this same region. N-terminal changes caused by the L68 mutants cluster mainly to residues forming CI2's α-helix, with the L68V mutant perturbing the N-terminal half of the helix (residues 30-36) and the L68A mutant perturbing nearly the whole helix. The I76V mutant, in contrast, perturbs the loop immediately prior to the start of the α-helix. The non-folding-nucleus mutants cause no perturbation of dynamics in these regions of the protein.

The C-terminal half of CI2 (approximately after residue 46) is perturbed by all mutants and generally becomes more flexible. It is also in this region where the greatest increases in flexibility ($\Delta S^2 \approx -0.1$) are to be found. In fact, many of the residues showing changes near -0.1 are the same across the various mutants. These residues include 49, 56, 60, 67, 69, 72, and 79, and are scattered throughout the protein's structure. The larger values of ΔS^2 for the residues are in almost all cases attributable to the selection of model 5 (S^2_{fast}, S^2_{slow}, $\tau_{e,\text{slow}}$) during data fitting, which indicates that the mutations all induce more complex backbone dynamics at these

residues that cannot be described by simpler forms of the spectral density that contain fewer parameters.

Collectively, the ^{15}N relaxation results indicate that CI2's backbone becomes slightly more flexible upon larger-to-smaller mutation of aliphatic side chains in the hydrophobic core. What distinguishes the various mutants from each other is their ability to perturb the N-terminal half of the protein main chain. Only the folding nucleus mutants (L68V, L68A, I76V) were able to affect the N-terminal half of the protein, with the effects localized to CI2's α-helix and the turn leading to it. The non-folding-nucleus core mutants were only able to perturb the C-terminal half of the protein, approximately after residue 46. Additionally, for all mutants, certain residues in the C-terminal half appear to undergo more complex dynamics, characterized by contributions from faster and slower ps-ns motions, than in the WT. We also note that initial CPMG-based ^{15}N relaxation-dispersion experiments (45) did not reveal the presence of any motions taking place on the μs-ms time scale for either WT CI2 or CI2 L68A (data not shown). While all core mutations were able to increase backbone flexibility on the ps-ns time scale, they apparently have no effect on the backbone in the μs-ms time regime. Information about CI2 backbone flexibility over very slow time scales (~ seconds) is available via hydrogen/ deuterium exchange (HX) experiments, and HX data have been used as restraints in computational models of the CI2 native state ensemble (46). From these simulations, it was determined that individual RMS residue fluctuations averaged over all members of the native ensemble are mostly constant over the entire primary sequence. The profile of the largest observed fluctuations per residue, however, distinctly reveals that CI2's α-helix is the most fluctuating unit of the whole structure. Furthermore, the largest-amplitude fluctuations in the native state ensemble were observed at residue A35 and immediately before residue I76, which are two of the three folding nucleus residues. Our study indicates that only the folding nucleus mutations were able to affect ps-ns flexibility throughout the whole protein. This is consistent with the notion that folding nucleus residues play an important role in the native state dynamics.

[2]H-Based Side-Chain Experiments Reveal that CI2's Hydrophobic Core is Uniquely Rigid

[15]N relaxation is an excellent method for determining the flexibility of protein backbones, but the behavior of the backbone is often distinct from the side chains (47). It is interesting to study side-chain dynamics, because side chains are involved in key protein functions such as catalysis and molecular recognition. Studying side-chain dynamics is thus a way to gain further insight into those phenomena. [2]H relaxation experiments applied to -CH_2D methyl isotopomers are excellent for obtaining information about the motional amplitudes and time scales of the methyl-bearing side chains in proteins. CI2 is particularly suited to analysis by these types of experiments because of the large number of methyl-containing side chains distributed throughout its structure. Thus, CI2 contains enough -CH_2D probes to reveal how core mutations affect ps-ns side-chain dynamics in all regions of the protein. Analogously to the ^{15}N relaxation studies, ^{2}H dynamics experiments lead to the calculation of S^2_{axis} and τ_e parameters for each methyl group. S^2_{axis} represents the amplitude of motion of the methyl group symmetry axis, and τ_e values as determined by ^{2}H relaxation are motional correlation times that contain contributions from rotation about and reorientation of the methyl symmetry axis, although the values are dominated by the former (30).

Historically, ^{2}H dynamics studies on methyl-bearing side chains have been conducted by measuring the relaxation of ^{2}H longitudinal (D_z) and transverse (D_+) magnetization as a function of time (33). One strength of the present study is that it expands our previous perturbation-response analyses of serine protease inhibitors (eglin c and CI2) by making use of three newer ^{2}H relaxation experiments in addition to the two original experiments. The major advantage of applying all five ^{2}H relaxation experiments (D_z, D_+, AP, QO, DQ) is that it enables

robust fitting of the relaxation data to a three-parameter form of the spectral density function, which in turn allows for identification of local nanosecond-scale dynamic processes (48).

Seven total ^{2}H relaxation measurements (D_z and D_+ at two fields; AP, DQ, QO at one field) were made for WT, L68V, L68A, I76V, and V66A. For V28A, only D_+ and D_z data at two fields are available, which precludes robust fitting to the three-parameter spectral density function. One complete and independent set of data was acquired for each of two separate samples of WT CI2, and the extracted S^2_{axis} and τ_e values were compared to one another. Figure 3 demonstrates that the results of the two independent analyses of WT CI2 side-chain dynamics show the expected lack of change, a control that increases confidence in the methodology before analyzing the dynamical perturbations in CI2 mutants. Changes in S^2_{axis} and τ_e between mutant and WT were calculated by subtracting the WT values from the mutant values. The ΔS^2_{axis} data can be found in Figure 4. Most striking is the overall pattern of changes when comparing each mutant to WT CI2. For nearly every methyl group, ΔS^2_{axis} is negative and falls in the range of -0.05 to -0.1, with an average value of approximately -0.06. This indicates that, for all mutants, the vast majority of methyl-containing side chains have become more flexible on the ps-ns time scale as a result of mutation, without regard either to the specific chemical nature of the mutation or its particular location within the hydrophobic core. This result mirrors the backbone dynamics results, but the significant increases in flexibility are more numerous and globally distributed for the side chains. Such globally-distributed, uniform changes in the amplitude of motion of nearly every detectable methyl group (Figure 5) were not observed either in similar studies of eglin c (49-51) or in mutants of the Fyn SH3 domain (52). Additionally, while the amplitudes of side-chain motion are all perturbed to a similar degree seemingly irrespective of the position of mutation, the time scales of motion (reflected in the parameter τ_e) are not affected to any great degree (representative data in Figure 4). It thus appears that the internal side-chain dynamics of WT CI2 are constrained at or modulated to a unique level of rigidity, such that mutations in the hydrophobic core result in a small but general perturbation to the physical determinants of side-chain dynamics, with the observable result being a global increase in side-chain flexibility. This global coupling of dynamics to the mutation of core residues is a novel experimental manifestation of cooperativity. CI2 is a classically non-allosteric protein, but if these changes in side-chain dynamics, particularly at the reactive loop, were to lead to a change in functional competency, this would by definition be an allosteric effect, and appropriate functional assays will be carried out in future studies.

It is important to note that we do not claim that the side chains of CI2 are abnormally rigid in an absolute sense, but rather that WT CI2's particular architecture and composition appear to support the dynamics of all the side chains such that any core perturbation "bumps" the side-chain dynamics away from the WT parameters to a nearly identical extent, as can be seen in Figure 6. These are each single mutants compared to WT CI2, but are *double* mutants compared to each other. Noticeably, there are many fewer significant differences in dynamics in this double mutant comparison than there are between either of the two single mutants and WT CI2, and many of the significant differences between the two single mutants cluster to the hydrophobic core. Furthermore, among the differences that do exist there are both increases and decreases in flexibility, which is in sharp contrast to the major behavior of the single mutants compared to the WT. The lack of many substantial differences among the side-chain dynamics of the various CI2 single mutants supports our conclusions that mutation seemingly anywhere in the hydrophobic core affects the global side-chain dynamics to a very similar degree.

Mutation to Putative Energetic Linchpin L68 Results in Increased "Slower" Motions at the Reactive Loop

The chief benefit of the expansive set of side-chain ^2H relaxation measurements obtained for each CI2 variant is the ability to detect the presence of "slower" nanosecond-scale motions that are not handled adequately by the standard two-parameter form of the spectral density. The data shown in Figure 4 resulted from model selection (two-parameter versus three-parameter spectral densities) for each methyl group in both WT CI2 and all mutants. Table 1 lists the methyl groups for which nanosecond-scale motions were detected in each variant; these methyl groups are marked with an asterisk in the panels of Figure 4. Except for one isoleucine, the side-chain dynamics of WT CI2 are adequately described by a two-parameter model in which the fitted motional correlation times are all on a time scale much faster than overall tumbling. This is also the case for mutants V66 and I76. The series of mutations at L68 (L→V→A) reveals clearly distinct behavior. As the length of the side chain at position 68 is decreased, more and more methyl groups appear to have a slower nanosecond-scale contribution to their dynamics. Especially for L68A, most of the residues which experience these nanosecond-scale motions in response to mutation are localized to the functional site of CI2, its reactive loop (residues 53-63). Whether these nanosecond-scale motions, which lead to increased rigidity (positive ΔS^2_{axis}), will impact any functional parameters such as binding affinity for or inhibitory ability towards serine proteases will be addressed in future studies. Taken together, the model-selected side-chain dynamics data suggest that L68 is unique among core residues, as suggested by previous work (22). Mutations at that position alone resulted in a noticeable presence of "slower" motions, and the number of methyl groups with such motions increased as the length of the side chain at position 68 decreased. It is conceivable that the changes in reactive loop dynamics reflect the loss of the "linchpin" connection between the loop and CI2's hydrophobic core.

Effects of Mutations on CI2 Structure

We desired to determine the extent to which any structural perturbations caused by the mutations might be responsible for the observed widespread changes in dynamics. Structural perturbation to the backbone was assessed by measuring N-H_N and C_α-H_α residual dipolar couplings (RDCs). RDCs are exquisitely sensitive to local environment, so any change in local structure should be readily detectable (except for pure translations in the frame of alignment). By comparing RDC data for mutants to WT data, we can assess the degree to which the backbones of the two variants are similar. Representative data are shown in Figure 7. The extremely high squared correlation coefficients for mutant/WT comparisons suggest that there are no gross structural perturbations caused by the mutations.

Side-chain structure was investigated for WT CI2 and the L68V and L68A mutants via measurement of three-bond scalar couplings between the backbone and side-chain γ-methyls (Val, Ile, Thr). From those measurements, we calculated χ_1 rotamer populations and compared mutant populations to those of the WT. Representative data are presented in Figure 8. Probing the populations of χ_1 rotameric states using scalar couplings also revealed that side-chain structure is generally conserved as well, with one notable exception. The V32 side chain (green dot in the figure) shows an increasing preference for the +60° rotamer over the 180° rotamer as the side chain at position 68 is shortened from L to V to A. The amplitudes and time scales of the ps-ns dynamics of the V32 side chain are relatively constant between the L68V and L68A, but the rotamer populations of V32 in both mutants show signs of motional averaging, as all three rotamers are populated to some degree. Scalar couplings (and thus rotamer populations) are sensitive to motions across many time scales; since the ps-ns dynamics at V32 are relatively insensitive to mutation but the rotamer populations show increasing changes with mutation, it is likely that some other, slower dynamic process is occurring at this residue. Examples of that type of dynamics were also found in protein L (53).

In addition to ruling out gross alterations to side-chain structure, the aggregate rotamer population data suggest that the increases in mutant CI2 side-chain flexibility occur *within* the energy wells of individual rotameric states and are not attributable to significantly increased rotamer sampling. It is known that rotameric transitions result in decreased S^2_{axis} values measured by NMR (54,55), but we do not observe significant changes in rotamer populations upon mutation, except for the single example discussed above. Thus, the global decrease in S^2_{axis} values observed for the CI2 mutants results not from increased transitioning among rotameric states, but rather from increased dynamics within individual rotamer energy wells.

Comparing CI2 Side-Chain Dynamics to the Homologue Eglin c

One particularly interesting open question in the field of protein dynamics is whether a given protein fold encodes the dynamics of its constituent amino acids and thus whether homologous proteins should have similar dynamics regardless of their sequence dissimilarity. By analyzing the CI2 dynamics data obtained in this study, we can contribute to the discussion of whether the dynamical character of proteins is encoded in the three-dimensional fold or whether local, sequence-specific considerations are more important. A large body of structure and dynamics information from NMR exists for the serine protease inhibitor eglin c (49,50), a homologue of CI2. Similar dynamical responses upon mutating the two proteins at equivalent positions argues that the overall fold is a major determinant of internal dynamics, whereas different consequences upon mutating equivalent positions argue that sequence-specific local effects are more important. Despite the host of NMR dynamics studies published in the literature, examples of direct comparisons of the side-chain dynamics of homologous proteins are comparatively lacking. Best *et al.* compared the side-chain dynamics of homologous fnIII domains from human fibronectin and human tenascin and found the side chains in the core of the tenascin fnIII domain to be much more flexible than those in the fibronectin domain; the increased flexibility of the tenascin fnIII side chains was attributed in part to both the amino acid composition and excess packing volume of the hydrophobic core (56). In contrast, other analyses of pooled side-chain dynamics data from numerous proteins suggest that, in general, there is little correlation between side-chain dynamics and structural properties such as depth of burial, solvent accessible surface area, packing density, or crystallographic B-factors (47).

Thus, we turned our attention to whether the side-chain dynamics of CI2 are similar to those of the homologue eglin c. Because the two proteins have different amino acids at structurally equivalent positions, the S^2_{axis} values were normalized to yield S^2_{norm} according to the method of Mittermaier *et al.* (57) in order to facilitate direct comparison. By calculating ΔS^2_{norm} for structurally equivalent positions in CI2 and eglin c, we can estimate the similarity of the side-chain dynamics at those positions. In addition to WT CI2 and WT eglin c, S^2_{axis} (and thus S^2_{norm}) data at pH 7 and 25 °C exist for the mutant pair comprised of CI2 I76V and eglin c V63A. ΔS^2_{norm} calculations for the WT/WT and mutant/mutant pairs are presented in Figure 9.

In order to interpret these data in terms of similarity of dynamics, it is important to appreciate what value of ΔS^2_{norm} might be expected for two proteins of no significant dynamical similarity. We approached this question by generating a Gaussian distribution of S^2_{norm} values centered at zero and having a standard deviation of one. We then selected 100,000 random pairs of S^2_{norm} values based on this Gaussian distribution, calculated the absolute value of ΔS^2_{norm} for each pair, and averaged over all the pairs to determine that two proteins of only random dynamical similarity can be expected to have a pairwise average $|\Delta S^2_{norm}|$ of approximately 1.13. This value is marked with a dashed line in Figure 9.

Our ability to compare CI2 and eglin c is limited by the small number of positions in the two proteins that are structurally equivalent and both occupied by amino acids with methyl-bearing side chains. While CI2 has a large number of such side chains, eglin c contains a larger degree

of aromatic side chains, and thus the number of positions available for direct comparison is limited. Based on the comparisons available, however, the average $|\Delta S^2_{norm}|$ for WT CI2 versus WT eglin c is approximately 0.83, while the average value for CI2 I76V versus eglin c V63A is 1.08. This suggests semi-quantitatively that there is greater similarity between the side-chain dynamics of WT CI2 and WT eglin c than would be expected at random and would seem to support the possibility that the protein fold, rather than the local environment, encodes the dynamics of its constituent amino acids. In fact, Figure 9 shows that most of the $|\Delta S^2_{norm}|$ values for WT CI2 and WT eglin are at worst near and at best significantly below the calculated average value for random similarity; were it not for the peculiar behavior at residue 27, the $|\Delta S^2_{norm}|$ average across all comparable methyl groups would be smaller than 0.83 and thus indicate an even greater degree of similarity between the side-chain dynamics of the two WT proteins. The CI2 I76V and eglin c V63A mutants, however, are hardly more than randomly dynamically related to one another. This supports our proposition that native CI2 side-chain dynamics, whatever their specific physical determinants, are regulated or constrained to a unique global level and that any core mutation perturbs the side-chain dynamics away from their norm. In essence, the CI2 core mutations rob the mutants of their characteristic dynamical "CI2-ness" such that the CI2 I76V mutant shares little more than random dynamical similarity with the homologous eglin c mutant. This also indicates that the determinants of side-chain dynamics act with some subtlety, since structural characterizations revealed that there are no gross backbone or side-chain structural perturbations upon mutating CI2 core residues. These conclusions are tentative on account of the lack of available dynamics data collected under the same experimental conditions for structurally homologous positions in CI2 and eglin c.

Conclusions

This paper presents the results of an extensive NMR study of the effects of hydrophobic core mutations in chymotrypsin inhibitor 2 on the internal dynamics of both the backbone and methyl-containing side-chains. The core mutations generally resulted in increased flexibility on the ps-ns time scale, but while the particular backbone results were mutant-dependent, the side chains showed the same slight but global increase in flexibility regardless of the position or chemical nature of the mutation. We suggest that the internal dynamics of WT CI2 are modulated in such a way as to be at some maximum of possible internal rigidity and that any small mutational perturbation in the core knocks the cohesive whole off balance, with the particular result being a small global increase in backbone and side-chain flexibility. Additionally, a progressive shortening of the L68 side chain leads to the increasing appearance of slower nanosecond-scale dynamics, primarily localized to the reactive loop. If it is indeed the case that L68 serves as a connection between the reactive loop and the hydrophobic core, as evidence in the literature suggests, then abolishing this link by shortening the side chain might decouple the behavior of the loop from the behavior of the hydrophobic core in the ps-ns time regime.

We have also performed an initial comparison of the degree of similarity in the side-chain dynamics of two homologues, CI2 and eglin c, for both the pair of WT proteins and a pair of structurally homologous mutants. The available data suggest that the ps-ns side-chain dynamics of WT CI2 and WT eglin c exhibit more than random similarity, while the dynamics of the mutant pair are no more similar than two random proteins would be. We interpret this idea in the context of alteration to the physical determinants of side-chain dynamics upon mutation, with the CI2 I76V mutation altering these determinants in such a way that the resultant side-chain dynamics are no longer characteristic of the WT protein. Thus the similarity in the side-chain dynamics of WT CI2 and WT eglin c is abolished upon mutating two proteins at the equivalent position. The dynamical similarity of the two WT proteins suggests the importance of a protein's fold in determining internal dynamics; however, the reduced degree of similarity in the side-chain dynamics of the homologous mutants suggests that some local, sequence-

dependent effect(s) from the mutations must also be contributing to the observed dynamics. Further investigation of the effects of mutation on the dynamics of homologous proteins is needed in order to clarify the relative importance of global and local influences in regulating the observed dynamics.

Acknowledgements

Abbreviations

AIC, Akaike's information criterion
AP, deuterium antiphase magnetization
BIC, Bayesian information criterion
CI2, chymotrypsin inhibitor 2
D_z, deuterium longitudinal magnetization
D_+, deuterium in-phase transverse magnetization
DQ, deuterium double quantum coherence
μs-ms, microsecond-to-millisecond
NMR, nuclear magnetic resonance
NOE, nuclear Overhauser enhancement
PCR, polymerase chain reaction
ps-ns, picosecond-to-nanosecond
QO, deuterium quadrupolar order
RDCs, residual dipolar couplings
S^2, generalized order parameter characterizing amplitude of N-H bond motions
S^2_{axis}, order parameter characterizing amplitude of methyl symmetry axis motions
τ_e, correlation time for internal motions
τ_m, a protein's global tumbling time
WT, wild-type

References

1. D'Aquino JA, Gomez J, Hilser VJ, Lee KH, Amzel LM, Freire E. The magnitude of the backbone conformational entropy change in protein folding. Proteins 1996;25:143–156. [PubMed: 8811731]

2. Yang D, Kay LE. Contributions to conformational entropy arising from bond vector fluctuations measured from NMR-derived order parameters: application to protein folding. J. Mol. Biol 1996;263:369–382. [PubMed: 8913313]

3. Zidek L, Novotny MV, Stone MJ. Increased protein backbone conformational entropy upon hydrophobic ligand binding. Nat. Struct. Biol 1999;6:1118–1121. [PubMed: 10581552]

4. Wrabl JO, Shortle D, Woolf TB. Correlation between changes in nuclear magnetic resonance order parameters and conformational entropy: molecular dynamics simulations of native and denatured staphylococcal nuclease. Proteins 2000;38:123–133. [PubMed: 10656260]

5. Stone MJ. NMR relaxation studies of the role of conformational entropy in protein stability and ligand binding. Acc. Chem. Res 2001;34:379–388. [PubMed: 11352716]

6. Wand AJ. Dynamic activation of protein function: a view emerging from NMR spectroscopy. Nat. Struct. Biol 2001;8:926–931. [PubMed: 11685236]

7. Bocharov EV, Korzhnev DM, Blommers MJ, Arvinte T, Orekhov VY, Billeter M, Arseniev AS. Dynamics-modulated biological activity of transforming growth factor beta3. J. Biol. Chem 2002;277:46273–46279. [PubMed: 12221089]

8. Johnson E, Chazin WJ, Rance M. Effects of calcium binding on the side-chain methyl dynamics of calbindin D9k: a 2H NMR relaxation study. J. Mol. Biol 2006;357:1237–1252. [PubMed: 16476440]

9. Frederick KK, Marlow MS, Valentine KG, Wand AJ. Conformational entropy in molecular recognition by proteins. Nature 2007;448:325–329. [PubMed: 17637663]

10. Cooper A, Dryden DTF. Allostery without conformational change: a plausible model. Eur. Biophys. J 1984;11:103–109. [PubMed: 6544679]

11. Li Z, Lukasik SM, Liu Y, Grembecka J, Bielnicka I, Bushweller JH, Speck NA. A mutation in the S-switch region of the Runt domain alters the dynamics of an allosteric network responsible for CBFbeta regulation. J. Mol. Biol 2006;364:1073–1083. [PubMed: 17059830]

12. Popovych N, Sun S, Ebright RH, Kalodimos CG. Dynamically driven protein allostery. Nat. Struct. Mol. Biol 2006;13:831–838. [PubMed: 16906160]

13. Eisenmesser EZ, Millet O, Labeikovsky W, Korzhnev DM, Wolf-Watz M, Bosco DA, Skalicky JJ, Kay LE, Kern D. Intrinsic dynamics of an enzyme underlies catalysis. Nature 2005;438:117–121. [PubMed: 16267559]

14. Watt ED, Shimada H, Kovrigin EL, Loria JP. The mechanism of rate-limiting motions in enzyme function. Proc. Natl. Acad. Sci. USA 2007;104:11981–11986. [PubMed: 17615241]

15. Ming D, Bruschweiler R. Prediction of methyl-side chain dynamics in proteins. J. Biomol. NMR 2004;29:363–368. [PubMed: 15213434]

16. Zhang F, Bruschweiler R. Contact model for the prediction of NMR N-H order parameters in globular proteins. J. Am. Chem. Soc 2002;124:12654–12655. [PubMed: 12392400]

17. McPhalen CA, James MN. Crystal and molecular structure of the serine proteinase inhibitor CI-2 from barley seeds. Biochemistry 1987;26:261–269. [PubMed: 3828302]

18. Svendsen I, Jonassen I, Hejgaard J, Boisen S. Amino acid sequence homology between a serine protease inhibitor from barley and potato I inhibitor. Carlsberg Res. Commun 1980;45:389–395.

19. Itzhaki LS, Otzen DE, Fersht AR. The structure of the transition state for folding of chymotrypsin inhibitor 2 analysed by protein engineering methods: evidence for a nucleation-condensation mechanism for protein folding. J. Mol. Biol 1995;254:260–288. [PubMed: 7490748]

20. Shakhnovich E, Abkevich V, Ptitsyn O. Conserved residues and the mechanism of protein folding. Nature 1996;379:96–98. [PubMed: 8538750]

21. Dokholyan NV, Li L, Ding F, Shakhnovich EI. Topological determinants of protein folding. Proc. Natl. Acad. Sci. USA 2002;99:8637–8641. [PubMed: 12084924]

22. Hilser VJ, Dowdy D, Oas TG, Freire E. The structural distribution of cooperative interactions in proteins: analysis of the native state ensemble. Proc. Natl. Acad. Sci. USA 1998;95:9903–9908. [PubMed: 9707573]

23. Muhandiram DR, Kay LE. Gradient-enhanced triple-resonance three-dimensional NMR experiments with improved sensitivity. J. Magn. Reson. Ser. A 1994;103:203–216.

24. Uhrín D, Uhrínová S, Leadbeater C, Nairn J, Price NC, Barlow PN. 3D HCCH$_3$-TOCSY for resonance assignment of methyl-containing side chains in ^{13}C-labeled proteins. J. Magn. Reson 2000;142:288–293. [PubMed: 10648145]

25. Neri D, Szyperski T, Otting G, Senn H, Wüthrich K. Stereospecific nuclear magnetic resonance assignments of the methyl groups of valine and leucine in the DNA-binding domain of the 434 repressor by biosynthetically directed fractional 13C labeling. Biochemistry 1989;28:7510–7516. [PubMed: 2692701]

26. Delaglio F, Grzesiek S, Vuister GW, Zhu G, Pfeifer J, Bax A. NMRPipe: a multidimensional spectral processing system based on UNIX pipes. J. Biomol. NMR 1995;6:277–293. [PubMed: 8520220]

27. Johnson BA, Blevins RA. NMRView: a computer program for the visualization and analysis of NMR data. J. Biomol. NMR 1994;4:603–614.

28. Farrow NA, Muhandiram R, Singer AU, Pascal SM, Kay CM, Gish G, Shoelson SE, Pawson T, Forman-Kay JD, Kay LE. Backbone dynamics of a free and phosphopeptide-complexed Src homology 2 domain studied by ^{15}N NMR relaxation. Biochemistry 1994;33:5984–6003. [PubMed: 7514039]

29. Lipari G, Szabo A. Model-free approach to the interpretation of nuclear magnetic resonance relaxation in macromolecules. 1. Theory and range of validity. J. Am. Chem. Soc 1982;104:4546–4559.

30. Lee AL, Flynn PF, Wand AJ. Comparison of ^{2}H and ^{13}C NMR Relaxation Techniques for the Study of Protein Methyl Group Dynamics in Solution. J. Am. Chem. Soc 1999;121:2891–2902.

31. Jarymowycz VA, Stone MJ. Fast time scale dynamics of protein backbones: NMR relaxation methods, applications, and functional consequences. Chem. Rev 2006;106:1624–1671. [PubMed: 16683748]

32. Chen J, Brooks CL III, Wright PE. Model-free analysis of protein dynamics: assessment of accuracy and model selection protocols based on molecular dynamics simulation. J. Biomol. NMR 2004;29:243–257. [PubMed: 15213423]

33. Muhandiram DR, Yamazaki T, Sykes BD, Kay LE. Measurement of ^{2}H T_1 and $T_{1\rho}$ Relaxation Times in Uniformly ^{13}C-Labeled and Fractionally ^{2}H-Labeled Proteins in Solution. J. Am. Chem. Soc 1995;117:11536–11544.

34. Millet O, Muhandiram DR, Skrynnikov NR, Kay LE. Deuterium spin probes of side-chain dynamics in proteins. 1. Measurement of five relaxation rates per deuteron in ^{13}C-labeled and fractionally ^{2}H-enriched proteins in solution. J. Am. Chem. Soc 2002;124:6439–6448. [PubMed: 12033875]

35. Chou JJ, Gaemers S, Howder B, Louis JM, Bax A. A simple apparatus for generating stretched polyacrylamide gels, yielding uniform alignment of proteins and detergent micelles. J. Biomol. NMR 2001;21:377–382. [PubMed: 11824758]

36. Ottiger M, Delaglio F, Bax A. Measurement of J and dipolar couplings from simplified two-dimensional NMR spectra. J. Magn. Reson 1998;131:373–378. [PubMed: 9571116]

37. Permi P. Measurement of residual dipolar couplings from ^{1}H$_\alpha$ to ^{13}C$_\alpha$ and ^{15}N using a simple HNCA-based experiment. J. Biomol. NMR 2003;27:341–349. [PubMed: 14512731]

38. Valafar H, Prestegard JH. REDCAT: A Residual Dipolar Coupling Analysis Tool. J. Magn. Reson 2004;167:228–241. [PubMed: 15040978]

39. Grzesiek S, Vuister GW, Bax A. A simple and sensitive experiment for measurement of J$_{CC}$ couplings between backbone carbonyl and methyl carbons in isotopically enriched proteins. J. Biomol. NMR 1993;3:487–493. [PubMed: 8400833]

40. Vuister GW, Wang AC, Bax A. Measurement of three-bond nitrogen-carbon *J*-couplings in proteins uniformly enriched in ^{15}N and ^{13}C. J. Am. Chem. Soc 1993;115:5334–5335.

41. Hennig M, Bermel W, Spencer A, Dobson CM, Smith LJ, Schwalbe H. Side-chain conformations in an unfolded protein: χ$_1$ distributions in denatured hen lysozyme determined by heteronuclear ^{13}C, ^{15}N NMR spectroscopy. J. Mol. Biol 1999;288:705–723. [PubMed: 10329174]

42. Schnell JR, Dyson HJ, Wright PE. Effect of cofactor binding and loop conformation on side chain methyl dynamics in dihydrofolate reductase. Biochemistry 2004;43:374–383. [PubMed: 14717591]

43. Luginbuhl P, Pervushin KV, Iwai H, Wuthrich K. Anisotropic molecular rotational diffusion in 15N spin relaxation studies of protein mobility. Biochemistry 1997;36:7305–7312. [PubMed: 9200679]

44. Lee LK, Rance M, Chazin WJ, Palmer AG 3rd. Rotational diffusion anisotropy of proteins from simultaneous analysis of 15N and 13C alpha nuclear spin relaxation. J. Biomol. NMR 1997;9:287–298. [PubMed: 9204557]

45. Loria JP, Rance M, Palmer AG. A Relaxation-Compensated Carr-Purcell-Meiboom-Gill Sequence for Characterizing Chemical Exchange by NMR Spectroscopy. J. Am. Chem. Soc 1999;121:2331–2332.

46. Best RB, Vendruscolo M. Structural interpretation of hydrogen exchange protection factors in proteins: characterization of the native state fluctuations of CI2. Structure 2006;14:97–106. [PubMed: 16407069]

47. Igumenova TI, Frederick KK, Wand AJ. Characterization of the fast dynamics of protein amino acid side chains using NMR relaxation in solution. Chem. Rev 2006;106:1672–1699. [PubMed: 16683749]

48. Skrynnikov NR, Millet O, Kay LE. Deuterium spin probes of side-chain dynamics in proteins. 2. Spectral density mapping and identification of nanosecond time-scale side-chain motions. J. Am. Chem. Soc 2002;124:6449–6460. [PubMed: 12033876]

49. Clarkson MW, Gilmore SA, Edgell MH, Lee AL. Dynamic coupling and allosteric behavior in a nonallosteric protein. Biochemistry 2006;45:7693–7699. [PubMed: 16784220]

50. Clarkson MW, Lee AL. Long-range dynamic effects of point mutations propagate through side chains in the serine protease inhibitor eglin c. Biochemistry 2004;43:12448–12458. [PubMed: 15449934]

51. Boyer JA, Lee AL. Monitoring Aromatic Picosecond to Nanosecond Dynamics in Proteins via ^{13}C Relaxation: Expanding Perturbation Mapping of the Rigidifying Core Mutation, V54A, in Eglin c. Biochemistry. 2008In press

52. Mittermaier A, Kay LE. The response of internal dynamics to hydrophobic core mutations in the SH3 domain from the Fyn tyrosine kinase. Protein Sci 2004;13:1088–1099. [PubMed: 15044737]

53. Millet O, Mittermaier A, Baker D, Kay LE. The effects of mutations on motions of side-chains in protein L studied by 2H NMR dynamics and scalar couplings. J. Mol. Biol 2003;329:551–563. [PubMed: 12767834]

54. Chou JJ, Case DA, Bax A. Insights into the Mobility of Methyl-Bearing Side Chains in Proteins from $^{3}J_{CC}$ and $^{3}J_{CN}$ Couplings. J. Am. Chem. Soc 2003;125:8959–8966. [PubMed: 12862493]

55. Hu H, Hermans J, Lee AL. Relating side-chain mobility in proteins to rotameric transitions: insights from molecular dynamics simulations and NMR. J. Biomol. NMR 2005;32:151–162. [PubMed: 16034666]

56. Best RB, Rutherford TJ, Freund SM, Clarke J. Hydrophobic core fluidity of homologous protein domains: relation of side-chain dynamics to core composition and packing. Biochemistry 2004;43:1145–1155. [PubMed: 14756550]

57. Mittermaier A, Davidson AR, Kay LE. Correlation between 2H NMR side-chain order parameters and sequence conservation in globular proteins. J. Am. Chem. Soc 2003;125:9004–9005. [PubMed: 15369343]
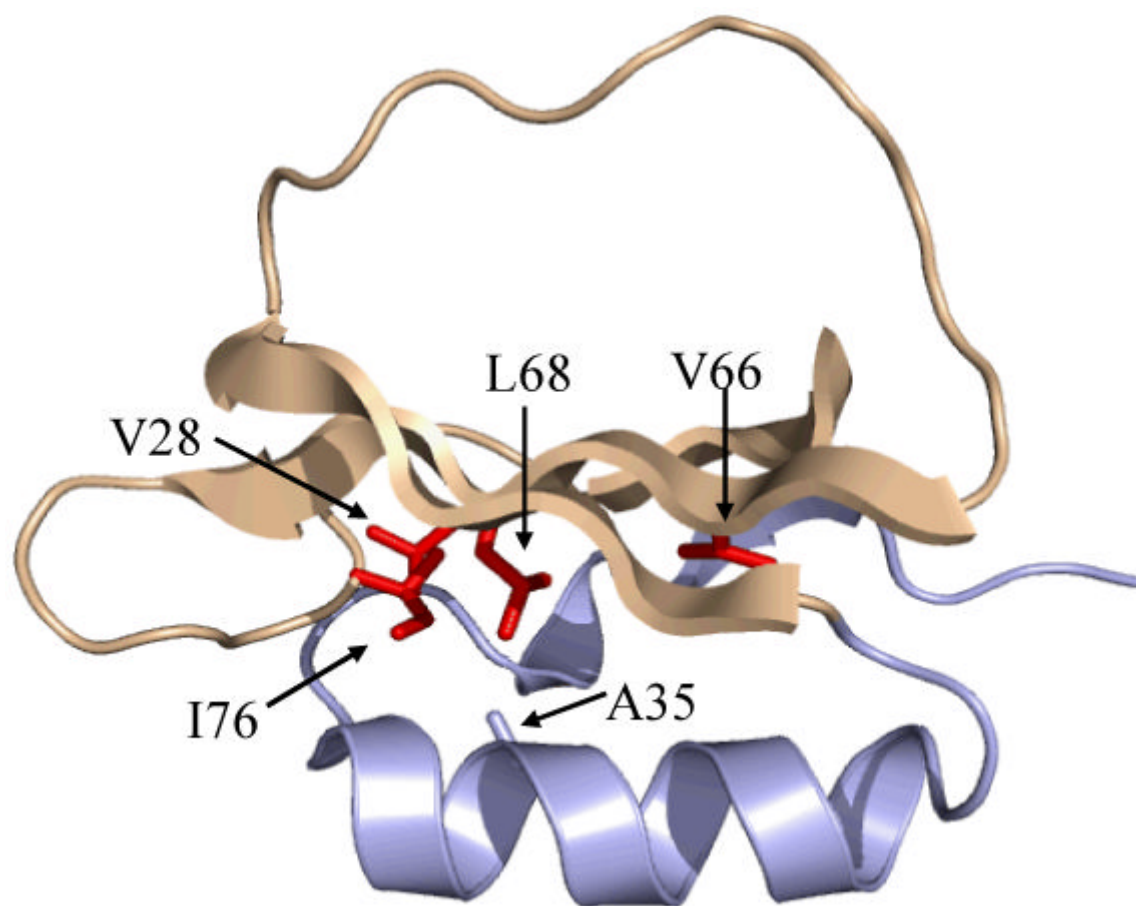
Figure 1.
The structure of chymotrypsin inhibitor 2 (PDB code 2CI2), with the sites of mutation examined in this study shown in red. The third canonical member of the CI2 folding nucleus, A35, has not been examined in this work and is shown in gray. The backbone coloring corresponds to the two distinct regions of dynamical perturbation (N-terminal region, light blue; C-terminal region, beige) revealed by ^{15}N relaxation experiments (see text).
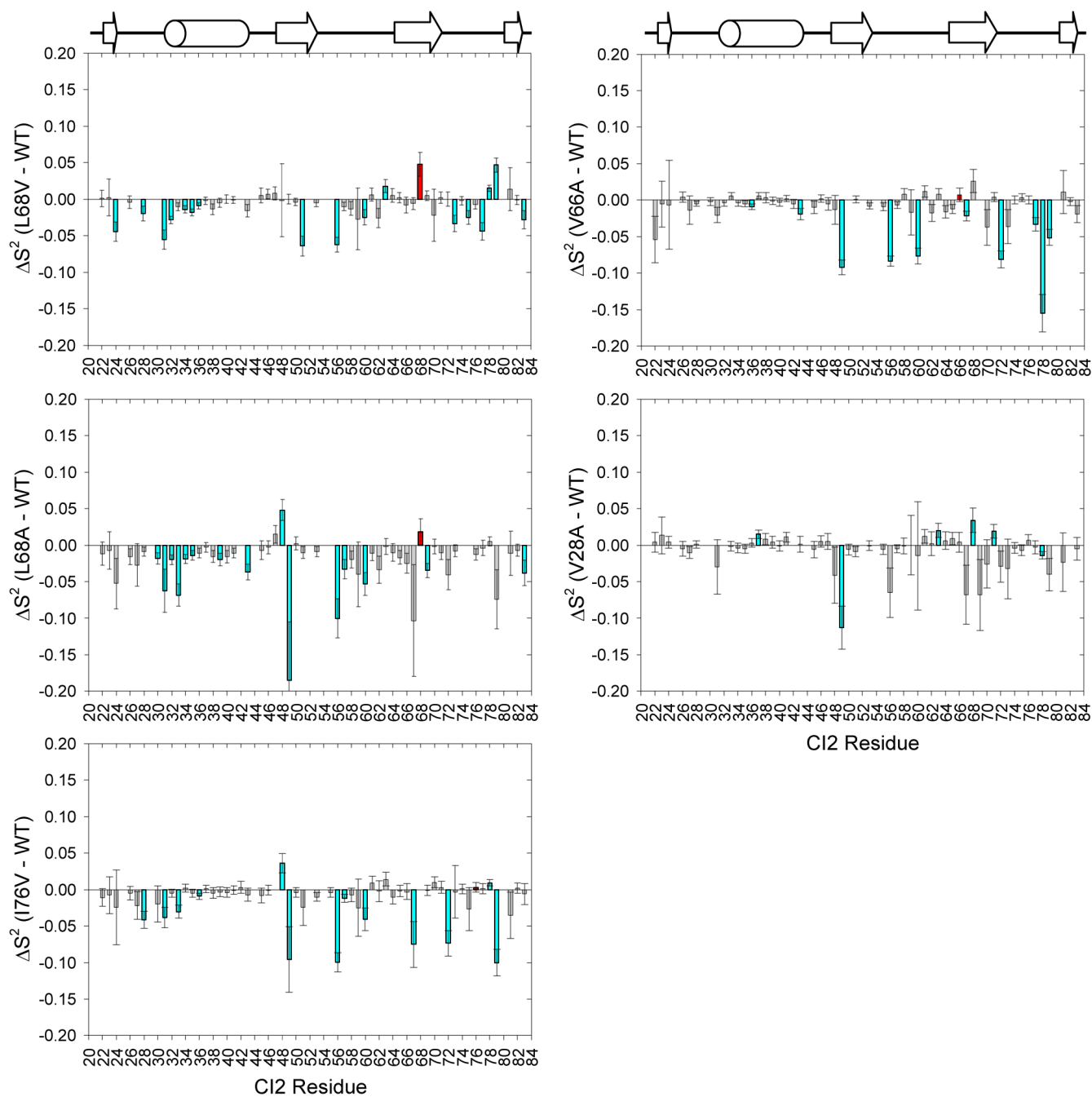
Figure 2.
Changes in the amplitude of backbone motions (ΔS^2) for the CI2 hydrophobic core mutants based on Lipari-Szabo model free analysis of ^{15}N relaxation data acquired at 25 °C. Plots in the left column are for folding nucleus mutants, whereas the right column shows data for core mutants that are not part of the canonical folding nucleus. In all plots, the site of mutation is indicated by a red bar, and residues exhibiting significant changes in dynamics are colored cyan.
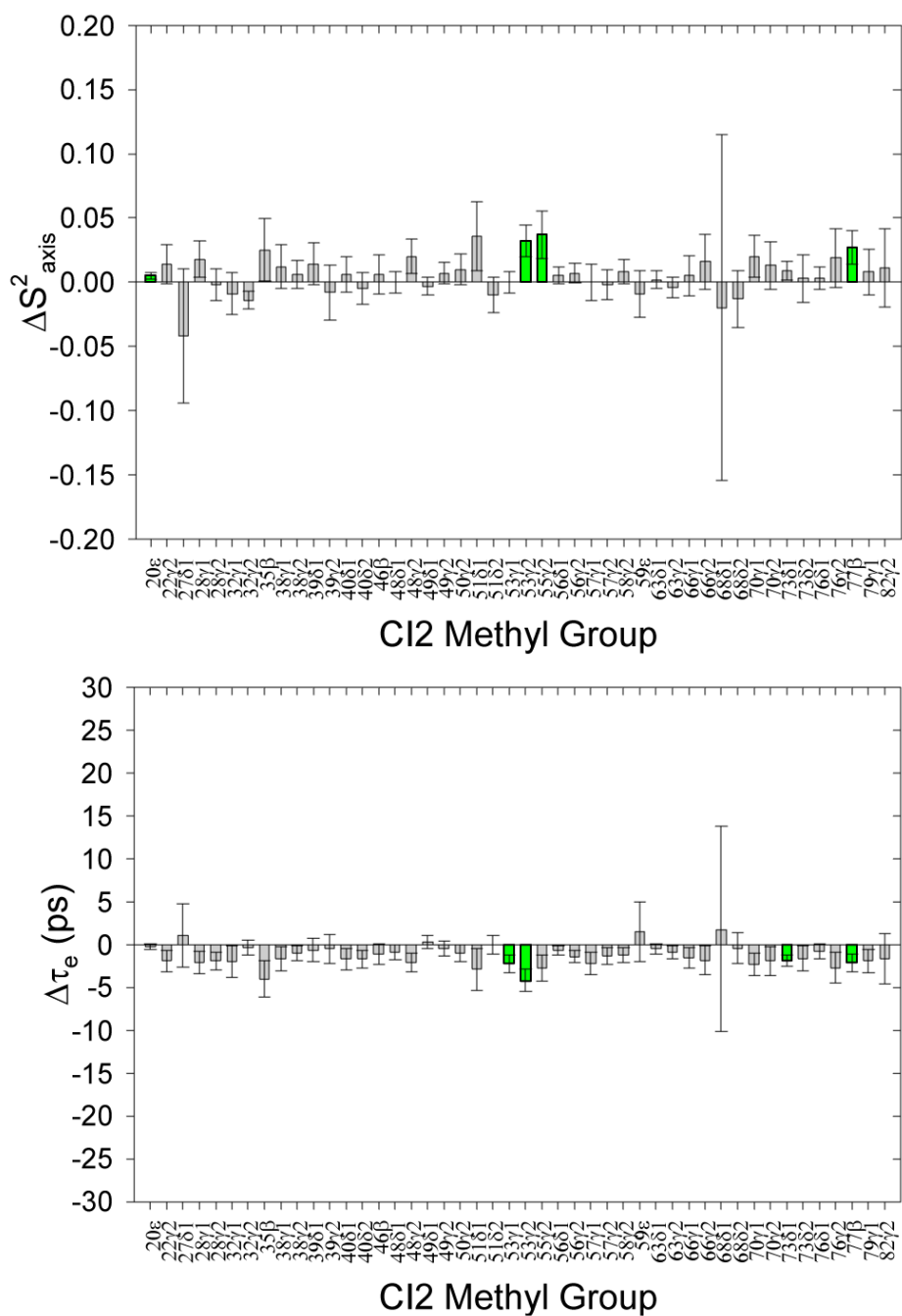
Figure 3.
Control analysis of side-chain model free dynamics parameters extracted from independent replicate ^2H relaxation measurements of different WT CI2 samples. For nearly every methyl group, the differences between the extracted S^2_{axis} and τ_e parameters for the two replicate sets of data are zero, within error. The very few small differences deemed significant are consistent with our 2σ standard and are colored green.
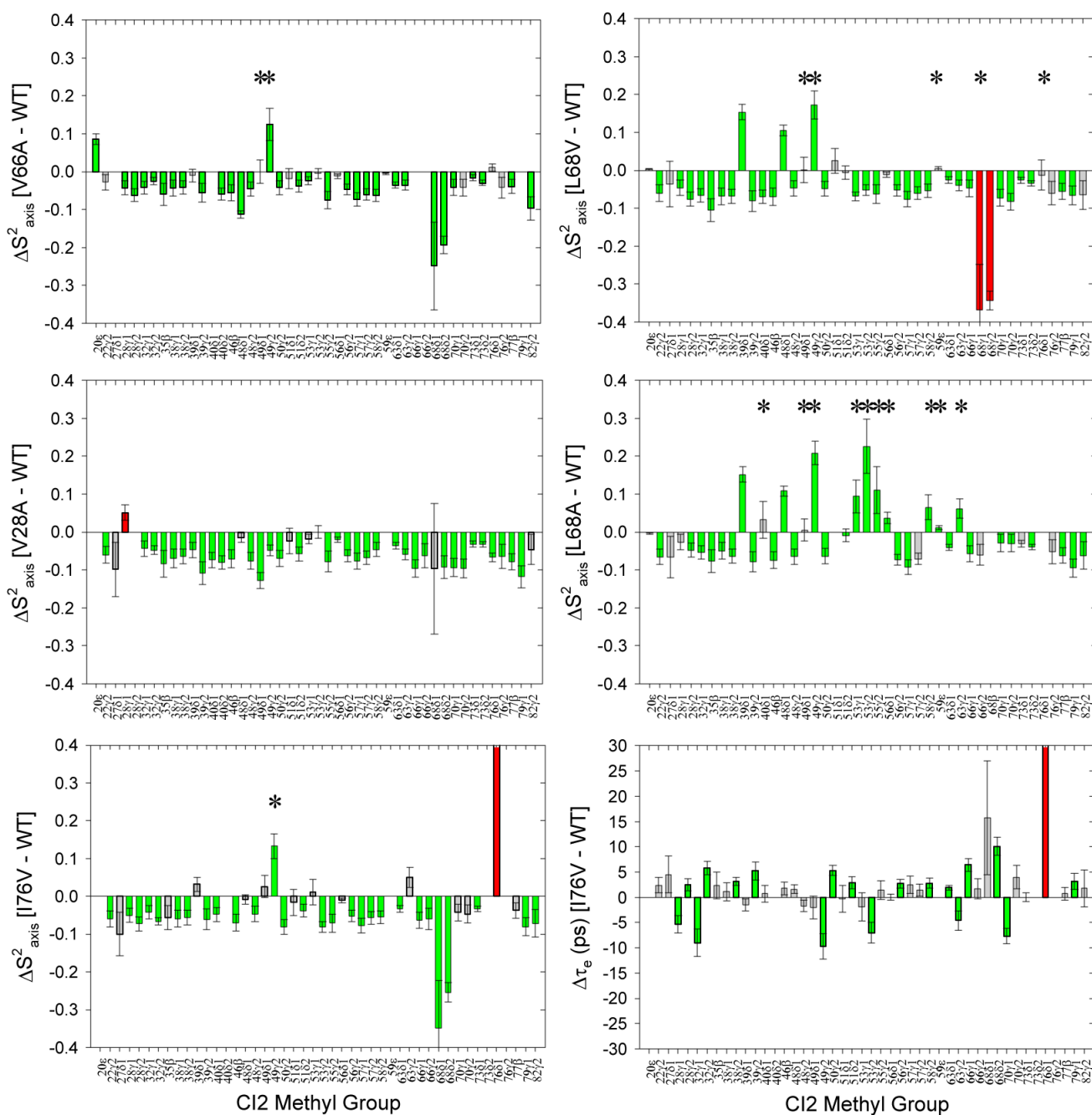
Figure 4.
^{2}H relaxation analysis of changes in the amplitudes of methyl-containing side-chain motions (ΔS^2_{axis}) with respect to WT CI2 for the hydrophobic core mutants studied. Green bars represent significant changes ($\geq 2\sigma$). Red bars represent the site of mutation, if data are available. The asterisks denote methyl groups experiencing slower nanosecond-scale motions based on LS-3 model selection during fitting of the relaxation data.
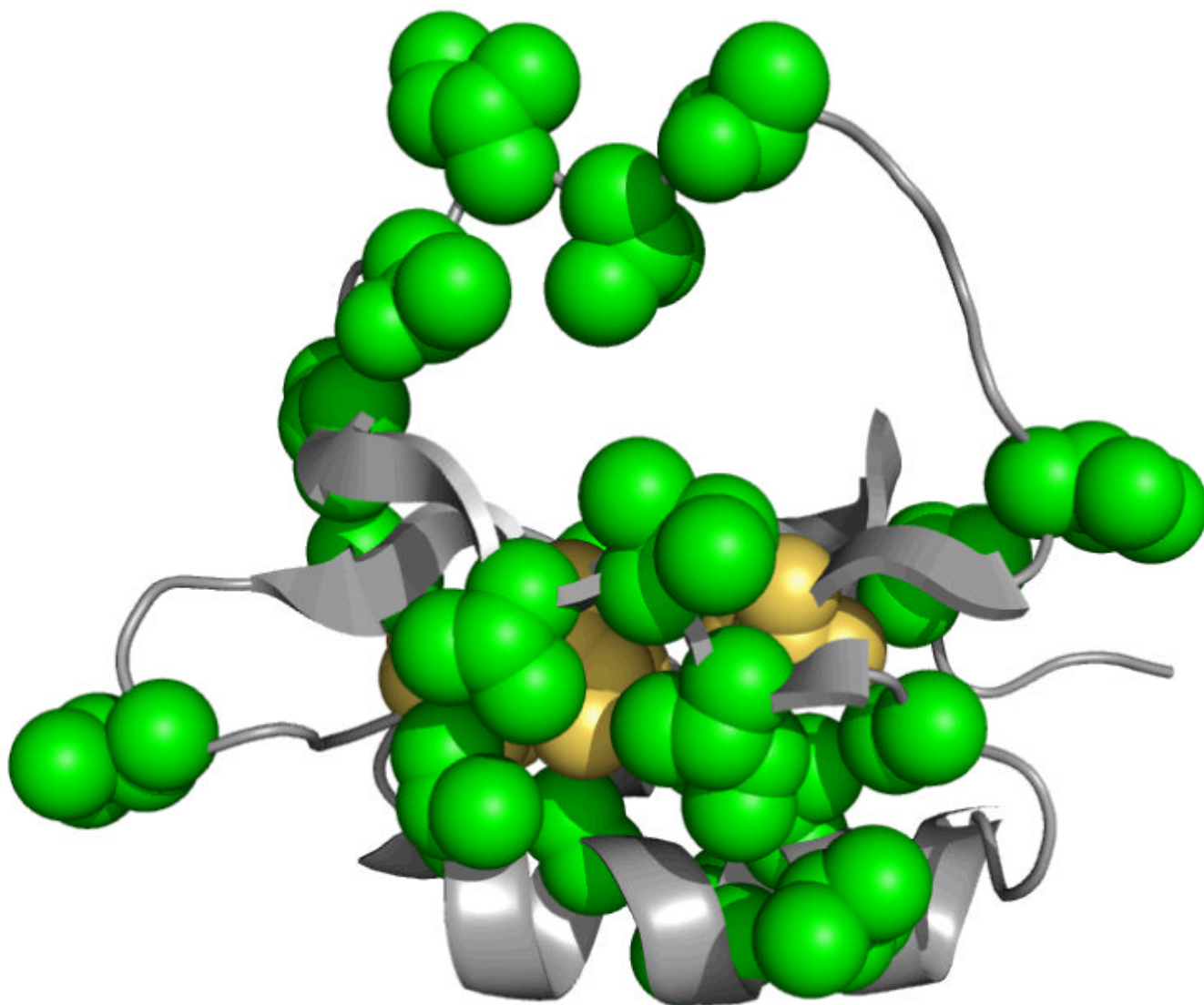
Figure 5.
A graphical summary of the ^{2}H side-chain dynamics results. In yellow are the sites of the individual single mutants (L68A, L68V, I76V, V66A, V28A). The green residues are those methyl-bearing side chains that have significant changes in S^2_{axis} in no fewer than 4 of the 5 single mutants investigated. Changes in the amplitude of side-chain motion radiate to all regions of the three dimensional structure and encompass nearly every methyl group which could be experimentally observed.
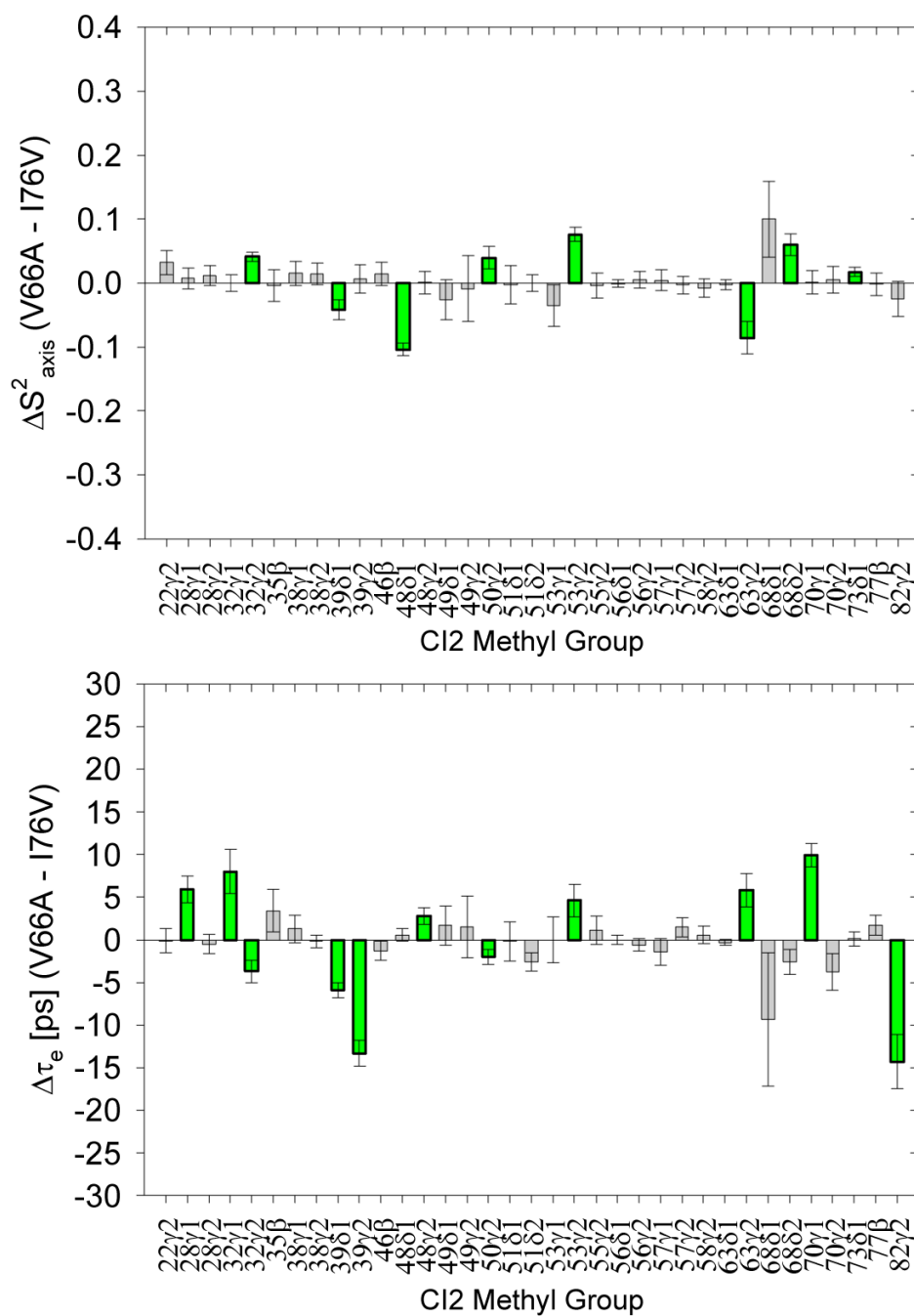
Figure 6.
A comparison of the side-chain dynamics of a "double mutant" pair comprised of CI2 I76V and CI2 V66A. The dynamics of these two mutants are much more similar to each other than either is to WT CI2.
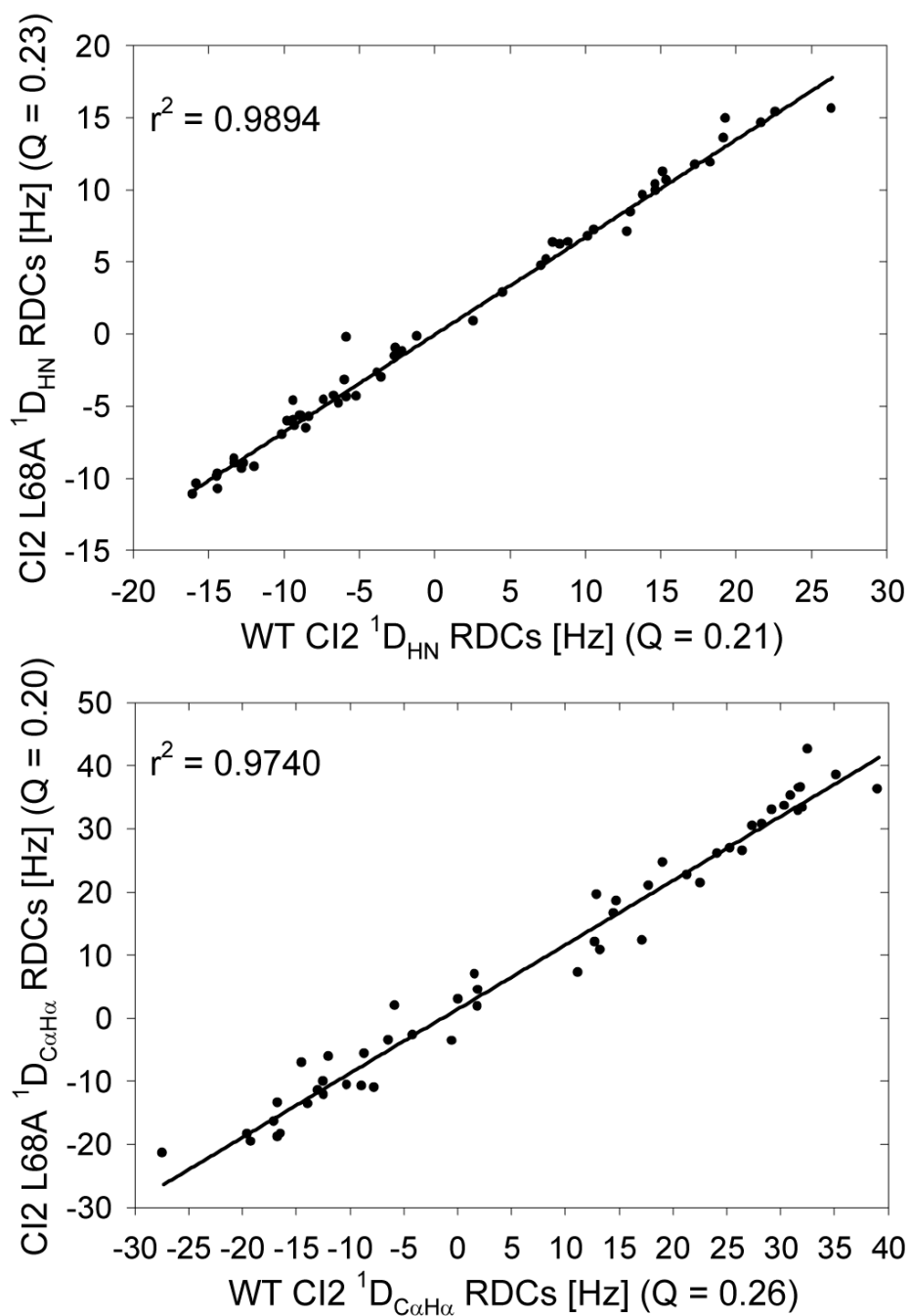
Figure 7.
A comparison of residual dipolar couplings (RDCs) for CI2 L68A versus WT CI2. Mutant N-H (top panel) and C^α-H^α (bottom panel) RDCs correlate extremely well with WT values, indicating that no significant structural rearrangements occur upon mutation. Q-factors for all variants were calculated using the WT CI2 structure. The correlations observed here are highly representative of the mutant/WT RDC comparisons for all mutants tested.
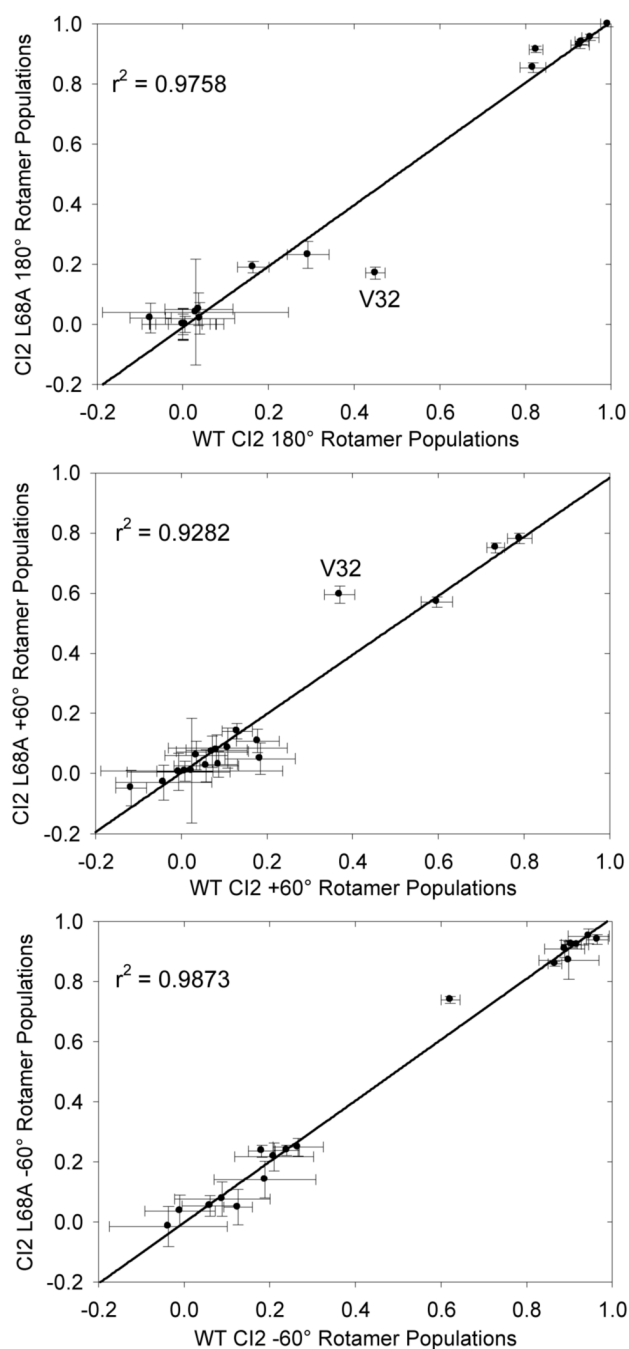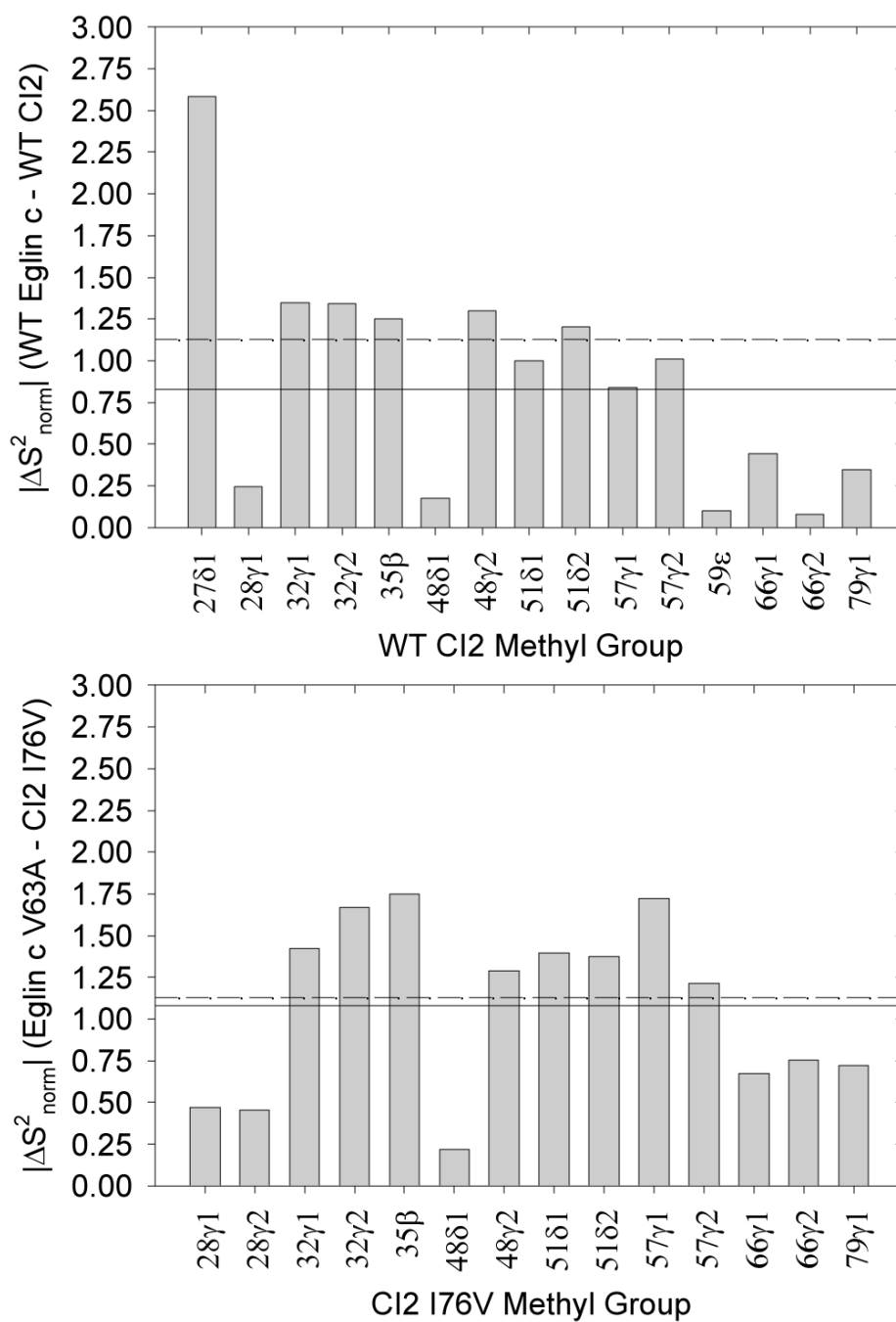
Figure 8.
A comparison of the χ_1 rotamer populations of WT CI2 and CI2 L68A calculated from three-bond scalar coupling measurements as a probe of side-chain structure. The populations of the three canonical rotameric states (+60°, -60°, 180°) are well conserved between WT CI2 and L68A, suggesting that the mutation does not grossly affect side-chain structure. The one significant exception is residue V32, which experiences a population shift from the major rotamer of 180° to the +60° rotamer as the side chain of residue 68 is progressively shortened.

Figure 9.
Comparisons of CI2 side-chain dynamics with respect to the homologue eglin c. Plotted are | ΔS^2_{norm}| values for WT CI2 vs. WT eglin c (top) and the homologous mutant pair CI2 I76V and eglin c V63A (bottom). The dashed line in both panels is | ΔS^2_{norm}| = 1.13, the pairwise average value expected if the two proteins shared no more than random dynamical similarity. The actual pairwise averages (solid lines) are | ΔS^2_{norm}| = 0.83 (top) and 1.08 (bottom).

Table 1

Selection of LS-3 model for CI2 mutants

Variant	Methyl Groups with Detected Nanosecond-Scale Motions
WT	$I49_\delta$
V66A	$I49_{\gamma2}$, $I49_\delta$
I76V	$I49_{\gamma2}$,
L68V	$I49_{\delta1}$, $I49_{\gamma2}$, $M59_\varepsilon$, $V68_{\delta1}$, $I76_{\delta1}$
L68A	$L40_{\delta1}$, $I49_{\delta1}$, $I49_{\delta2}$, $V53_{\gamma1}$, $V53_{\gamma2}$, $T55_{\gamma2}$, $I56_{\delta1}$, $T58_{\gamma2}$, $M59_\varepsilon$, $I63_{\gamma2}$, $V79_{\gamma2}$